Cell PRESS

Open ACCESS

Cell Reports

Report

Thermodynamic Stabilization of the Folded Domain of Prion Protein Inhibits Prion Infection in Vivo

Qingzhong Kong,[1,*] Jeffrey L. Mills,[2,3,4] Bishwajit Kundu,[2,3,5] Xinyi Li,[1,3,6] Liuting Qing,[1,3] Krystyna Surewicz,[2] Ignazio Cali,[1] Shenghai Huang,[1] Mengjie Zheng,[1] Wieslaw Swietnicki,[2,7] Frank D. Sönnichsen,[2,8] Pierluigi Gambetti,[1] and Witold K. Surewicz[2,*]

[1]Department of Pathology, Case Western Reserve University, Cleveland, OH 44106, USA

[2]Department of Physiology and Biophysics, Case Western Reserve University, Cleveland, OH 44106, USA

[3]These authors contributed equally to this work

[4]Present address: Department of Chemistry, The State University of New York at Buffalo, Buffalo, NY 14260, USA

[5]Present address: Kusuma School of Biological Sciences, Indian Institute of Technology, Hauz Khas, New Delhi 110016, India

[6]Present address: Department of Molecular and Experimental Medicine, The Scripps Research Institute, La Jolla, CA 92037, USA

[7]Present address: Department of Biotechnology, Wroclaw Research Center EIT+, 54-066 Wroclaw, Poland

[8]Present address: Otto Diels Institute for Organic Chemistry, Christian Albrechts University, 24098 Kiel, Germany

*Correspondence: qxk2@case.edu (Q.K.), witold.surewicz@case.edu (W.K.S.)

http://dx.doi.org/10.1016/j.celrep.2013.06.030

SUMMARY

Prion diseases, or transmissible spongiform encephalopathies (TSEs), are associated with the conformational conversion of the cellular prion protein, PrP^{C}, into a protease-resistant form, PrP^{Sc}. Here, we show that mutation-induced thermodynamic stabilization of the folded, α-helical domain of PrP^{C} has a dramatic inhibitory effect on the conformational conversion of prion protein in vitro, as well as on the propagation of TSE disease in vivo. Transgenic mice expressing a human prion protein variant with increased thermodynamic stability were found to be much more resistant to infection with the TSE agent than those expressing wild-type human prion protein, in both the primary passage and three subsequent subpassages. These findings not only provide a line of evidence in support of the protein-only model of TSEs but also yield insight into the molecular nature of the $PrP^{C} \rightarrow PrP^{Sc}$ conformational transition, and they suggest an approach to the treatment of prion diseases.

INTRODUCTION

Transmissible spongiform encephalopathies (TSEs) are a group of neurodegenerative disorders that include Creutzfeldt-Jakob disease in humans, scrapie in sheep, chronic wasting disease in cervids, and bovine spongiform encephalopathy in cattle (Aguzzi and Polymenidou, 2004; Caughey et al., 2009; Cobb and Surewicz, 2009; Collinge, 2001; Prusiner, 1998; Weissmann, 2004). The prion hypothesis asserts that the transmission of TSEs does not require nucleic acids, and that the infectious TSE agent is proteinaceous in nature, consisting of a misfolded form of prion protein (PrP) (Prusiner, 1982). Once heretical, this protein-only model is now supported by a growing body of evidence, most notably due to the recent success in generating infectious prions in vitro from brain-derived (Castilla et al., 2005; Deleault et al., 2007) or bacterially expressed (Kim et al., 2010; Legname et al., 2004; Makarava et al., 2010; Wang et al., 2010) PrP. However, the mechanisms involved in the conformational conversion of the normal (cellular) PrP (denoted PrP^{C}) to the misfolded conformer (denoted PrP^{Sc}) remain largely unknown, hindering our understanding of the molecular basis of prion diseases as well as the development of therapeutic approaches.

Cellular human PrP^{C} is a glycoprotein that consists of an unstructured N-terminal region and a folded C-terminal domain comprised of three α helices and two very short β strands (Zahn et al., 2000). Conversion of this protein to an abnormal PrP^{Sc} isoform occurs by a posttranslational process involving a major conformational change that results in an increased proportion of β structure (Caughey et al., 1991; Pan et al., 1993). Although the three-dimensional structure of PrP^{Sc} remains unknown, a body of evidence suggests that this conformational transition involves at least partial refolding of the helix-rich C-terminal domain (Cobb et al., 2007; Govaerts et al., 2004; Smirnovas et al., 2011). This, together with recent findings that mutations that reduce the thermodynamic stability of PrP^{C} greatly increase the propensity of PrP^{C} to undergo a conversion to oligomeric β-sheet forms in vitro (Apetri et al., 2005; Vanik and Surewicz, 2002), prompted us to search for amino acid substitutions that stabilize the native α-helical structure, with the expectation that, if the protein-only hypothesis is correct, such mutations should suppress the $PrP^{C} \rightarrow PrP^{Sc}$ conversion and thus attenuate replication of the infectious prion agent.

RESULTS AND DISCUSSION

A particularly dramatic increase in thermodynamic stability of PrP^{C} was found upon replacement of valine (V) at position 209

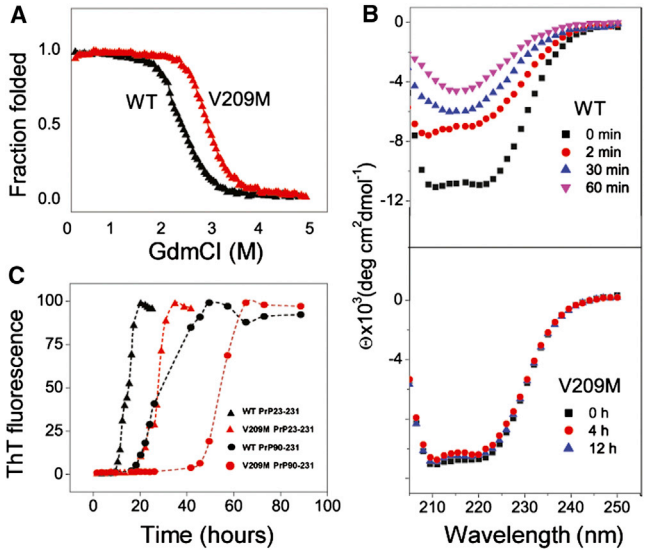

Figure 1. Effect of the V209M Mutation on the Biophysical Properties of Human PrP

(A) GdmCl-induced equilibrium unfolding for wild-type (WT) full-length human PrP (HuPrP23-231) and the V209M variant. The unfolding curves were obtained in 50 mM phosphate buffer, pH 7.

(B) Time-dependent transition of WT HuPrP90-231 and the V209M variant from α-helical structure to β-sheet oligomers as monitored by circular dichroism spectroscopy. Spectra were recorded in 50 mM sodium acetate, pH 4, in the absence of the denaturant and at different time points after the addition of 1 M GdmCl. The spectrum of the α-helical monomer shows a characteristic "double minimum" at ~210 and 220 nm, whereas the spectrum of β-sheet oligomers is characterized by lower intensity and a broad minimum around 215 nm.

(C) Time course of amyloid fibril formation for WT HuPrP and the V209M variant as monitored by thioflavine T fluorescence. Data for both full-length protein (HuPrP23-231) and HuPrP90-231 are shown. The lag phases (mean ± SD) based on three to four experiments are 6.5 ± 0.5 and 16.3 ± 1.4 hr for HuPrP23-231 and V209M HuPrP23-231, respectively, and 18 ± 2 and 42 ± 3 hr for HuPrP90-231 and V209M HuPrP90-231, respectively. See also Figure S1.

with methionine (M). As shown in Figure 1A, equilibrium unfolding of the full-length wild-type recombinant human PrP (HuPrP23-231) in guanidinium chloride (GdmCl) at pH 7 is characterized by a midpoint unfolding GdmCl concentration of 2.1 M and a free-energy difference between the native and unfolded states, ΔG^{o}, of 20.6 kJ/mol. For the V209M variant, the unfolding curve is shifted to much higher denaturant concentrations (midpoint at 2.8 M) and the ΔG^{o} value is increased to 31.9 kJ/mol. A similar effect was observed for N-truncated HuPrP90-231, with ΔG^{O} increasing from 20.9 to 30.0 kJ/mol. The observed increase of ~10 kJ/mol in the free energy of unfolding is remarkably high and, to the best of our knowledge, is among the largest reported for a single residue mutation in any protein. Thermodynamic stabilization of the native PrP structure by the Val209→Met substitution was further confirmed by thermal unfolding experiments using differential scanning calorimetry (Figure S1).

It was previously shown that under mildly acidic conditions in the presence of low concentrations of GdmCl, the N-truncated recombinant HuPrP90-231 undergoes a transition to an oligomeric β-sheet structure mimicking certain properties of PrP^{Sc} (Apetri et al., 2005; Vanik and Surewicz, 2002). Under the present experimental conditions (sodium acetate buffer, pH 4, 1 M GdmCl, protein concentration of 24 μM), the α-helix→β-sheet transition for the wild-type HuPrP90-231 was completed within ~60 min. In contrast, the V209M mutant was highly resistant to this conversion, remaining in a monomeric α-helical form even after 12 hr of incubation under identical conditions (Figure 1B).

Incubation of the recombinant PrP in the presence of GdmCl at neutral pH is known to result in the formation of thioflavine T-positive amyloid structures with fibrillar morphology (Apetri et al., 2005; Baskakov, 2004). Under the present experimental conditions, the conversion to amyloid fibrils for the wild-type HuPrP23-231 was characterized by a lag phase of 6.5 ± 0.5 hr. Again, upon replacement of Val209 with Met, this reaction became much slower, with an increased lag phase of 16.3 ± 1.4 hr (Figure 1C). For the N-truncated HuPrP90-231, the conversion reactions were slower compared with the full-length protein. However, also in this case the V209M mutation reduced the rate of the conversion reaction (lag phase of 18 ± 2 and 42 ± 3 hr for wild-type HuPrP90-231 and V209M HuPrP90-231, respectively; Figure 1C). Collectively, these data demonstrate that the V209M mutation greatly increases the thermodynamic stability of PrP^{C}, resulting in a remarkably reduced propensity of the protein to undergo a conversion to PrP^{Sc}-mimicking, β-sheet-rich aggregates in vitro.

An inspection of nuclear magnetic resonance (NMR) data indicates that the structure of wild-type human PrP (Zahn et al., 2000) is characterized by the presence of three cavities (PDB ID: 1QM0). Two of these cavities (with volumes of 57 and 14 $Å^3$ and surface areas of 76 and 29 $Å^2$) are surrounded by residues of the second and third α-helices and the loops connecting α-helix 1 with β strands 1 and 2 (Figure 2). The third cavity (18 $Å^3$, 34 $Å^2$) is located at the packing interface of helices 1 and 3. The presence of such cavities within the hydrophobic core of proteins is known to have a destabilizing effect (Eriksson et al., 1992). Our initial modeling suggested that the substitution of Met in place of Val 209 should largely eliminate the cavities in PrP, providing a rationale for improved thermodynamic stability. This prediction was verified by the NMR-determined structure (Figures 2 and S2; Table S1). Indeed, as shown in Figure 2, the structure of the V209M variant shows remarkably improved packing within the hydrophobic core, resulting in a complete removal of the two larger cavities near residue 209. This is a consequence of the different side-chain geometry of residue 209 and subtle changes in the packing and geometry of helices 1 and 3. Apart from this minor difference, the overall fold of the mutant protein remains unaltered.

To test whether thermodynamic stabilization of the folded domain of PrP is sufficient to confer resistance to prion replication in vivo, we created two lines of transgenic mice in the Friend Virus B (FVB)/PrP null background: one expressing wild-type human PrP [denoted Tg(HuPrP)] and the other expressing the superstable variant [denoted Tg($HuPrP^{V209M}$)]. Western blot analysis indicates that both lines of transgenic mice express PrP in the brain at a level similar to that observed for wild-type FVB mice, and with comparable electrophoretic profiles dominated by the diglycosylated form (Figures 3A and 3C). Confocal microscopy of primary neurons derived from Tg(HuPrP) and Tg($HuPrP^{V209M}$) mice (Figure 3B), as well as of human

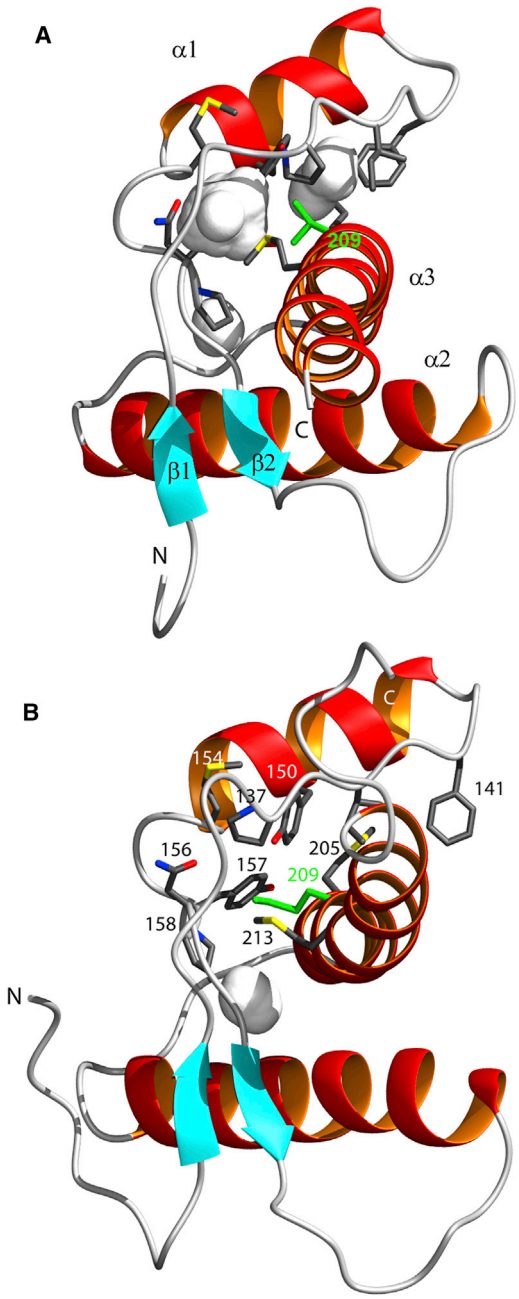

Figure 2. NMR-Determined Structures—Ribbon Representations—of the PrP Folded Domain

(A) Wild-type human PrP (Zahn et al., 2000; PDB ID: 1QM0).

(B) The V209M variant of human PrP. In the WT protein, two cavities (displayed as white spheres) are present near residue V209. In the V209M variant, these cavities are eliminated as a result of altered side-chain geometry of residue 209 and subtle changes in the packing and geometry of helices α1 and α3. A third cavity of nearly equal size in both proteins is found near Pro 158 between helices α2 and α3. Side chains surrounding the cavities are shown and labeled with residue numbers. The structure shown for the V209M variant represents the lowest-energy structure of the ensemble of 20 water-refined conformers. Additional structural details and statistics are provided in Figure S2 and Table S1.

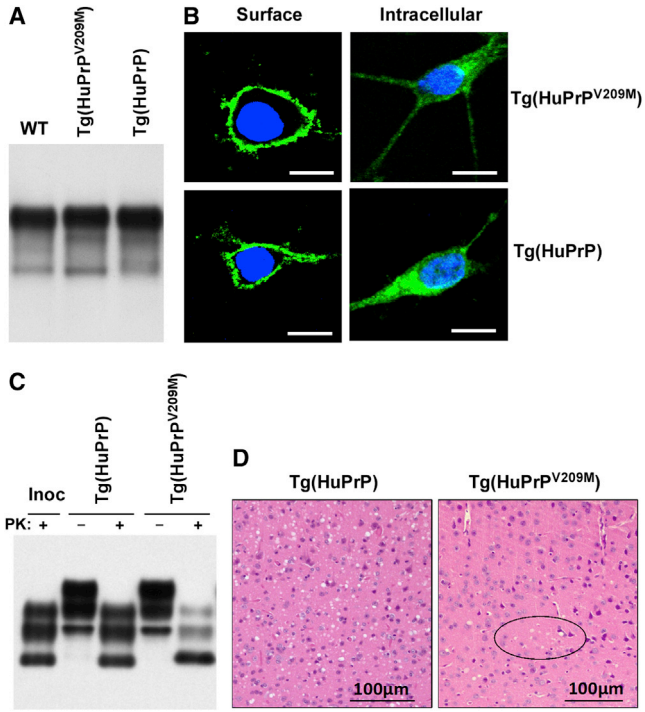

Figure 3. Transmission of CJD Prions in Tg(HuPrP) and Tg(HuPrP^{V209M}) Mice

(A) PrP expression levels in brains of Tg(HuPrP), Tg(HuPrP^{V209M}), and WT FVB mice as probed by western blotting using mAb 8H4.

(B) Cell-surface and intracellular localization of PrP in primary neurons prepared from Tg(HuPrP^{V209M}) and Tg(HuPrP) mice. Cells were probed for PrP with mAb 3F4, counterstained for nuclei with Hoechst, and examined with a confocal microscope. Scale bars: 10 μm.

(C) PrP^{Sc} in brains of sCJDMM1-infected Tg(HuPrP) and Tg(HuPrP^{V209M}) mice. Transgenic mice were intracerebrally inoculated with brain homogenate from a subject with sCJDMM1. Brain homogenates from symptomatic mice and the inoculum (Inoc) were subjected to western blot analysis with mAb 3F4 before (–) and after (+) PK treatment.

(D) Spongiform degeneration in brains of sCJDMM1-infected Tg(HuPrP) and Tg(HuPrP^{V209M}) mice. Fixed brain sections from cerebral cortex of Tg(HuPrP^{V209M}) mice show small and scattered areas with vacuoles (circled area), whereas in Tg(HuPrP) mice spongiform degeneration is much more widespread and severe. Brain sections were stained with hematoxylin and eosin. Scale bars: 100 μm. See also Figure S3.

neuroblastoma cell line M17 transfected with either wild-type human PrP (HuPrP) or the V209M variant (HuPrP^{V209M}) (data not shown), demonstrates that HuPrP and HuPrP^{V209M} have similar cellular distributions, residing both at the cell surface and in intracellular compartments. Furthermore, treatment of M17 cells expressing PrP^{V209M} with phosphatidylinositol-specific phospholipase C (PI-PLC) released HuPrP^{V209M} into the culture medium, indicating that, like wild-type PrP, PrP^{V209M} is attached to the cell membrane by a glycosylphosphatidylinositol (GPI) anchor (Figure S3). Together, these data indicate that Tg(HuPrP) and Tg(HuPrP^{V209M}) mice express comparable amounts of PrP, and that the cellular localization of PrP^{V209M} is indistinguishable from that of the wild-type protein.

After intracerebral inoculation with brain homogenates derived from subjects with sporadic Creutzfeldt-Jacob disease (sCJD),

Table 1. Primary and Secondary Transmissions of sCJD in Transgenic Mice

Tg Line	Inoculum	Attack Rate	Incubation Time (Days)[a]	Titers (ID_{50} U/g)
Tg(HuPrP)	sCJDMM1[b]	9/9	263 ± 13	4.6×10^7
	sCJDMM2[b]	9/9	267 ± 17	3.2×10^7
Tg($HuPrP^{V209M}$)	sCJDMM1	2/6	685, 696	
	sCJDMM2	0/7	≥798	
Tg(HuPrP)	Tg($HuPrP^{V209M}$)-passaged sCJDMM1	5/5	316 ± 16	8.3×10^5
Tg($HuPrP^{V209M}$)	Tg($HuPrP^{V209M}$)-passaged sCJDMM1	6/6	431 ± 30	
Tg(HuPrP)	sCJDMM1 passaged twice in Tg($HuPrP^{V209M}$)	7/7	267 ± 12[c]	
Tg($HuPrP^{V209M}$)	sCJDMM1 passaged twice in Tg($HuPrP^{V209M}$)	7/7	366 ± 18[e]	
Tg(HuPrP)	sCJDMM1 passaged thrice in Tg($HuPrP^{V209M}$)	10/10	295 ± 7[c]	
Tg($HuPrP^{V209M}$)	sCJDMM1 passaged thrice in Tg($HuPrP^{V209M}$)	4/6[d]	399 ± 6[e]	

See also Figure S4.
[a]Average values and SEMs are shown.
[b]The MM1 and MM2 subtypes of sCJD according to the classification of Parchi et al. (1999).
[c]The difference in incubation times between the third and fourth passages in Tg(HuPrP) mice is statistically insignificant (p = 0.11).
[d]Two mice are still alive with no apparent symptoms (at ~580 days postinoculation).
[e]The difference in incubation times between the third and fourth passages in Tg(HuV209MPrP) mice is statistically insignificant (p = 0.28).

all inoculated Tg(HuPrP) mice fell ill after an incubation time of ~263 days (Table 1), exhibiting classical symptoms of TSE disease. In sharp contrast, only two of six sCJDMM1-inoculated Tg($HuPrP^{V209M}$) mice (and none of seven sCJDMM2-inoculated Tg($HuPrP^{V209M}$) mice) became symptomatic after a very long incubation time of nearly 700 days (Table 1). As expected, western blot analysis revealed that the brains of all inoculated Tg(HuPrP) mice accumulated relatively large quantities of proteinase K (PK)-resistant PrP, PrP^{Sc}, which electrophoretically reproduced the pattern of the original sCJD PrP^{Sc} (Figure 3C). In contrast, PrP^{Sc} was found in the brains of only two symptomatic Tg($HuPrP^{V209M}$) mice, but not in the remaining 11 symptom-free animals, even after sodium phosphotungstate precipitation treatment of brain homogenate to enrich PrP^{Sc} (Safar et al., 1998). The electrophoretic profile of PrP^{Sc} from the two infected Tg($HuPrP^{V209M}$) mice differed from that of Tg(HuPrP) mice with regard to gel mobility and the ratio of bands representing different PrP^{Sc} glycoforms (Figure 3C). Furthermore, compared with the inoculated Tg(HuPrP) mice, the two affected Tg($HuPrP^{V209M}$) mice displayed much less severe overall spongiform neurodegeneration, reduced PrP immunostaining, and significantly different lesion profiles (Figures 3D and S4A–S4D). Altogether, these data indicate that, compared with transgenic mice expressing wild-type human PrP, Tg($HuPrP^{V209M}$) mice are more resistant to infection with sCJD prions. However, the question must be raised as to whether the enhanced resistance of Tg($HuPrP^{V209M}$) mice is intrinsic or due to the "mutation barrier" related to the mismatch in the amino acid sequence between the wild-type sCJD PrP^{Sc} of the inoculum and the mutated PrP^{V209M} expressed by the recipient Tg($HuPrP^{V209M}$) mice.

The availability of two sCJD-affected Tg($HuPrP^{V209M}$) mice provided us with the opportunity to probe this question by performing a second passage experiment. Upon inoculation with the Tg($HuPrP^{V209M}$)-adapted sCJD preparations (which contained only the newly generated $PrP^{Sc(V209M)}$ isoform), all of the Tg(HuPrP) mice (which express wild-type PrP^{C}) became infected with an average incubation of 316 days, which is longer than the 263 days of incubation needed after inoculation of the original (not passaged) sCJD preparation (Table 1). This increase in incubation time most likely can be attributed to the mutation barrier now existing between the PrP^{V209M} of the inoculum and the PrP^{C} expressed by the recipient Tg(HuPrP) mice. Remarkably, despite the lack of any mutation barrier between the inoculum and Tg($HuPrP^{V209M}$) mice in this second-passage experiment, the Tg($HuPrP^{V209M}$) mice required a much longer incubation of ~431 days, although this time all of them succumbed to the disease (Table 1). Because the passage of prions in mutant mice might be associated with the strain adaptation phenomenon (Bartz et al., 2000), we performed two additional passages. Although the incubation time in the third passage in Tg($HuPrP^{V209M}$) mice decreased from 431 to 366 days, no further reduction in the incubation time was observed in the fourth passage, indicating that the adaptation process had been completed. Importantly, even at this point, the incubation time was still much longer for Tg($HuPrP^{V209M}$) mice than for Tg(HuPrP) mice (366 and 399 days versus 267 and 295 days in the third and fourth passages, respectively; Table 1). Thus, these data clearly demonstrate an inherently high resistance of Tg($HuPrP^{V209M}$) mice to sCJD prion infection.

Intriguingly, second- to fourth-passage Tg(HuPrP) mice inoculated with $PrP^{Sc(V209M)}$ were characterized by PrP^{Sc} electrophoretic patterns and lesion profiles that were indistinguishable from those observed in the first passage experiment with sCJD-inoculated Tg(HuPrP) mice, whereas distinct electrophoretic characteristics of $PrP^{Sc(V209M)}$ and lesion profiles were consistently maintained in passages in Tg($HuPrP^{V209M}$) mice (Figures S4C–S4E). These data strongly suggest that the PrP^{Sc} isoforms associated with the V209M mutation can be faithfully propagated only in the host containing this mutation, whereas in Tg(HuPrP) mice they "adapt back" to the characteristics apparently dictated by the wild-type PrP host.

Tg($HuPrP^{V209M}$) mice were specifically generated to test whether thermodynamic stabilization of the folded domain of

PrP^C as observed in vitro is sufficient to inhibit prion replication in vivo. The answer to this question is clearly yes, providing a line of evidence in support of the protein-only model of TSEs. While the requirement for PrP^C in TSE pathogenesis has been demonstrated in seminal experiments with PrP-knockout mice (Büeler et al., 1993), the present data show that this requirement is directly related to the ability of PrP^C to undergo a conversion to the PrP^{Sc} state, and that prion propagation in vivo can be effectively inhibited by stabilizing the normal α-helical conformation of PrP^C. Given the similar electronic and hydrophobic properties of Val and Met residues, it is highly unlikely that the reduced conversion propensity of the mutant protein is due to factors other than thermodynamic stabilization. Furthermore, since residue 209 is buried within the hydrophobic interior of the protein, its substitution should not affect the interaction of PrP^C with other cellular cofactors in vivo.

The finding that thermodynamic stabilization of the native α-helical domain of PrP^C inhibits prion propagation in mice impacts the ongoing debate regarding critical yet still unresolved issues in prion research: the mechanism of PrP conversion and the structure of the infectious PrP^{Sc} conformer. Although some models postulate that the C-terminal region of PrP^{Sc} retains at least partial native α-helical structure of PrP^C (DeMarco and Daggett, 2004; Govaerts et al., 2004), recent data indicate that PrP conversion involves major refolding of the entire C-terminal region, and that this region in PrP^{Sc} consists of β strands and short turns/loops, with no α helices present (Smirnovas et al., 2011). The present finding is consistent with the latter scenario, providing strong support to the notion that PrP conversion in vivo involves a major rearrangement of the α-helical domain of PrP^C.

Finally, the present data suggest a strategy for pharmacological intervention in prion diseases. Although a number of immuno- and chemotherapeutic approaches have been proposed (Cashman and Caughey, 2004), there is currently no effective treatment for TSEs. A promising new strategy has recently emerged, based on the downregulation of PrP^C expression using small interfering RNA (Pfeifer et al., 2006). However, this approach may carry significant risks given the reported role of PrP^C in cell signaling, neuroprotection, and other physiological processes (Westergard et al., 2007). The finding that one can effectively reduce prion replication in vivo by stabilizing the native conformation of PrP^C without manipulating its expression level offers an alternative and potentially more practical strategy based on screening and/or rational design of small molecules that can thermodynamically stabilize the normal conformation of monomeric PrP^C. Recently, a generally similar approach was successfully used to develop a clinically effective drug against transthyretin amyloidosis, even though in the latter case the stabilization is kinetic rather than thermodynamic, preventing dissociation of the transthyretin tetramer (Bulawa et al., 2012).

EXPERIMENTAL PROCEDURES

Protein Purification

Recombinant human PrP 90-231 (HuPrP90-231) and the V209M mutant (both 129M variants) were prepared and purified as described previously (Apetri et al., 2005). Uniformly ^{15}N- and $^{13}C/^{15}N$-labeled proteins for NMR spectroscopy were expressed in *Escherichia coli* using a minimal medium containing $^{13}C_6$ glucose (3 g/l) and/or ^{15}N NH_4Cl (1 g/l) as the sole carbon and nitrogen sources, respectively.

Biophysical Experiments

Equilibrium unfolding experiments were performed with the use of circular dichroism spectroscopy (50 mM phosphate buffer, pH 7) by monitoring GdmCl-induced changes in ellipticity at 220 nm as described previously (Apetri et al., 2005). The unfolding curves were analyzed using a two-state transition model (Santoro and Bolen, 1988). The conversion of PrP variants to β-sheet oligomers was performed in 50 mM sodium acetate buffer containing 1 M GdmCl, pH 4, and monitored by circular dichroism spectroscopy as described previously (Apetri et al., 2005). The concentration of each protein in these experiments was 24 μM. The conversion of the proteins to amyloid fibrils at neutral pH (50 mM phosphate buffer, 1.5 M GdmCl, pH 7, protein concentration of 30 μM) was performed and monitored by thioflavine T assay as described previously (Apetri et al., 2005).

Structural Studies

The structure of V209M human PrP was determined by NMR spectroscopy. Details of these experiments are provided in Extended Experimental Procedures.

Transgenic Mice

HuPrP and $HuPrP^{V209M}$ transgene constructs were based on the murine half-genomic PrP clone (HGPRP) (Fischer et al., 1996). Tg40, a Tg(HuPrP) line that expresses wild-type human PrP-129M at the same level as the murine PrP in wild-type FVB mice, was described previously (Kong et al., 2005). Tg($HuPrP^{V209M}$) mice were created in the same fashion and bred with FVB/$Prnp^{0/0}$ mice to obtain Tg($HuPrP^{V209M}$)$Prnp^{0/0}$ mice. The transgene expression in brain was examined by western blotting analysis using monoclonal antibody (mAb) 3F4 or 8H4 as described below. Tg20, a Tg($HuPrP^{V209M}$) line expressing the mutant PrP at the wild-type FVB mouse level, was used for all transmission experiments. All transgenic mice used were in the $Prnp^{o/o}$ background.

Inoculation and Examination of Transgenic Mice

Frozen brain tissues from human subjects with sCJD or prion-infected transgenic mice were homogenized in PBS and inoculated intracerebrally into the brains of Tg(HuPrP) and Tg($HuPrP^{V209M}$) mice as previously described (Kong et al., 2005). Thirty microliters of 1% brain homogenate was injected into each animal. Prion symptoms were monitored as previously described (Kong et al., 2005) and the animals were sacrificed within 2–3 days after the appearance of symptoms. Each brain was sliced sagittally; half was frozen for western blot analysis (see below) and half was fixed in formalin for staining with hematoxylin and eosin or anti-PrP antibody 3F4 (Castellani et al., 1996; Kong et al., 2005). The prion titers of the sCJD or mouse brain tissues were calculated according to the incubation time using a previously described method based on endpoint titration of sCJDMM1 in Tg40 mice (Prusiner et al., 1982).

Western Blotting Analysis and Detection of PK-Resistant PrP

Total protein concentrations of brain homogenates in the lysis buffer (100 mM Tris, 150 mM NaCl, 0.5% Nonidet P-40, 0.5% sodium deoxycholate, 10 mM EDTA, pH 7.8) were measured with BCA Protein Assay Reagents (Thermo Fisher Scientific). Total PrP and PK-resistant PrP^{Sc} were examined by western blotting using precast SDS-PAGE gels with 8H4 or 3F4 antibodies in conjunction with horseradish-peroxidase-conjugated goat anti-mouse IgG Fc antibody essentially as described previously (Pan et al., 2001). PK digestion was performed for 1 hr at 37°C using 100 μg/ml of the enzyme.

Confocal Immunofluorescence Imaging of Primary Neurons

Primary cortical neuron cultures were prepared from day 14–16 embryos of Tg(HuPrP) and Tg($HuPrP^{V209M}$) mice (Yuan et al., 2008). Cell-surface and intracellular PrP was examined with a Zeiss LSM510 inverted confocal microscope using mAb 3F4 and goat anti-mouse IgG (H^+L) conjugated with highly cross-absorbed Alexa Fluor 488 (Invitrogen) as described previously (Mishra et al., 2002).

ACCESSION NUMBERS

The coordinates and structural restraints for V209M HuPrP have been deposited under BMRB accession number 19268, RCSB ID code rcsb103353, and PDB ID code 2M8T.

SUPPLEMENTAL INFORMATION

Supplemental Information includes Extended Experimental Procedures, four figures, and one table and can be found with this article online at http://dx.doi.org/10.1016/j.celrep.2013.06.030.

ACKNOWLEDGMENTS

We are grateful to B. Chakraborty, F. Chen, M. Wang, L. Wang, D. Kofsky, P. Wang, K. Edmonds, K. Chen, M. Payne, A. Dutta, and S. Chen for their technical assistance and M. Buck for critical reading of the manuscript. This study was supported by National Institutes of Health grants NS044158, NS038604, NS052319, and AG014359.

Received: December 20, 2011
Revised: May 29, 2013
Accepted: June 21, 2013
Published: July 18, 2013

REFERENCES

Aguzzi, A., and Polymenidou, M. (2004). Mammalian prion biology: one century of evolving concepts. Cell *116*, 313–327.

Apetri, A.C., Vanik, D.L., and Surewicz, W.K. (2005). Polymorphism at residue 129 modulates the conformational conversion of the D178N variant of human prion protein 90-231. Biochemistry *44*, 15880–15888.

Bartz, J.C., Bessen, R.A., McKenzie, D., Marsh, R.F., and Aiken, J.M. (2000). Adaptation and selection of prion protein strain conformations following interspecies transmission of transmissible mink encephalopathy. J. Virol. *74*, 5542–5547.

Baskakov, I.V. (2004). Autocatalytic conversion of recombinant prion proteins displays a species barrier. J. Biol. Chem. *279*, 7671–7677.

Büeler, H., Aguzzi, A., Sailer, A., Greiner, R.A., Autenried, P., Aguet, M., and Weissmann, C. (1993). Mice devoid of PrP are resistant to scrapie. Cell *73*, 1339–1347.

Bulawa, C.E., Connelly, S., Devit, M., Wang, L., Weigel, C., Fleming, J.A., Packman, J., Powers, E.T., Wiseman, R.L., Foss, T.R., et al. (2012). Tafamidis, a potent and selective transthyretin kinetic stabilizer that inhibits the amyloid cascade. Proc. Natl. Acad. Sci. USA *109*, 9629–9634.

Cashman, N.R., and Caughey, B. (2004). Prion diseases—close to effective therapy? Nat. Rev. Drug Discov. *3*, 874–884.

Castellani, R., Parchi, P., Stahl, J., Capellari, S., Cohen, M., and Gambetti, P. (1996). Early pathologic and biochemical changes in Creutzfeldt-Jakob disease: study of brain biopsies. Neurology *46*, 1690–1693.

Castilla, J., Saá, P., Hetz, C., and Soto, C. (2005). In vitro generation of infectious scrapie prions. Cell *121*, 195–206.

Caughey, B., Baron, G.S., Chesebro, B., and Jeffrey, M. (2009). Getting a grip on prions: oligomers, amyloids, and pathological membrane interactions. Annu. Rev. Biochem. *78*, 177–204.

Caughey, B.W., Dong, A., Bhat, K.S., Ernst, D., Hayes, S.F., and Caughey, W.S. (1991). Secondary structure analysis of the scrapie-associated protein PrP 27-30 in water by infrared spectroscopy. Biochemistry *30*, 7672–7680.

Cobb, N.J., and Surewicz, W.K. (2009). Prion diseases and their biochemical mechanisms. Biochemistry *48*, 2574–2585.

Cobb, N.J., Sönnichsen, F.D., McHaourab, H., and Surewicz, W.K. (2007). Molecular architecture of human prion protein amyloid: a parallel, in-register beta-structure. Proc. Natl. Acad. Sci. USA *104*, 18946–18951.

Collinge, J. (2001). Prion diseases of humans and animals: their causes and molecular basis. Annu. Rev. Neurosci. *24*, 519–550.

Deleault, N.R., Harris, B.T., Rees, J.R., and Supattapone, S. (2007). Formation of native prions from minimal components in vitro. Proc. Natl. Acad. Sci. USA *104*, 9741–9746.

DeMarco, M.L., and Daggett, V. (2004). From conversion to aggregation: protofibril formation of the prion protein. Proc. Natl. Acad. Sci. USA *101*, 2293–2298.

Eriksson, A.E., Baase, W.A., Zhang, X.J., Heinz, D.W., Blaber, M., Baldwin, E.P., and Matthews, B.W. (1992). Response of a protein structure to cavity-creating mutations and its relation to the hydrophobic effect. Science *255*, 178–183.

Fischer, M., Rülicke, T., Raeber, A., Sailer, A., Moser, M., Oesch, B., Brandner, S., Aguzzi, A., and Weissmann, C. (1996). Prion protein (PrP) with amino-proximal deletions restoring susceptibility of PrP knockout mice to scrapie. EMBO J. *15*, 1255–1264.

Govaerts, C., Wille, H., Prusiner, S.B., and Cohen, F.E. (2004). Evidence for assembly of prions with left-handed beta-helices into trimers. Proc. Natl. Acad. Sci. USA *101*, 8342–8347.

Kim, J.I., Cali, I., Surewicz, K., Kong, Q., Raymond, G.J., Atarashi, R., Race, B., Qing, L., Gambetti, P., Caughey, B., and Surewicz, W.K. (2010). Mammalian prions generated from bacterially expressed prion protein in the absence of any mammalian cofactors. J. Biol. Chem. *285*, 14083–14087.

Kong, Q., Huang, S., Zou, W., Vanegas, D., Wang, M., Wu, D., Yuan, J., Zheng, M., Bai, H., Deng, H., et al. (2005). Chronic wasting disease of elk: transmissibility to humans examined by transgenic mouse models. J. Neurosci. *25*, 7944–7949.

Legname, G., Baskakov, I.V., Nguyen, H.O., Riesner, D., Cohen, F.E., DeArmond, S.J., and Prusiner, S.B. (2004). Synthetic mammalian prions. Science *305*, 673–676.

Makarava, N., Kovacs, G.G., Bocharova, O., Savtchenko, R., Alexeeva, I., Budka, H., Rohwer, R.G., and Baskakov, I.V. (2010). Recombinant prion protein induces a new transmissible prion disease in wild-type animals. Acta Neuropathol. *119*, 177–187.

Mishra, R.S., Gu, Y., Bose, S., Verghese, S., Kalepu, S., and Singh, N. (2002). Cell surface accumulation of a truncated transmembrane prion protein in Gerstmann-Straussler-Scheinker disease P102L. J. Biol. Chem. *277*, 24554–24561.

Pan, K.M., Baldwin, M., Nguyen, J., Gasset, M., Serban, A., Groth, D., Mehlhorn, I., Huang, Z., Fletterick, R.J., Cohen, F.E., et al. (1993). Conversion of alpha-helices into beta-sheets features in the formation of the scrapie prion proteins. Proc. Natl. Acad. Sci. USA *90*, 10962–10966.

Pan, T., Colucci, M., Wong, B.S., Li, R., Liu, T., Petersen, R.B., Chen, S., Gambetti, P., and Sy, M.S. (2001). Novel differences between two human prion strains revealed by two-dimensional gel electrophoresis. J. Biol. Chem. *276*, 37284–37288.

Parchi, P., Giese, A., Capellari, S., Brown, P., Schulz-Schaeffer, W., Windl, O., Zerr, I., Budka, H., Kopp, N., Piccardo, P., et al. (1999). Classification of sporadic Creutzfeldt-Jakob disease based on molecular and phenotypic analysis of 300 subjects. Ann. Neurol. *46*, 224–233.

Pfeifer, A., Eigenbrod, S., Al-Khadra, S., Hofmann, A., Mitteregger, G., Moser, M., Bertsch, U., and Kretzschmar, H. (2006). Lentivector-mediated RNAi efficiently suppresses prion protein and prolongs survival of scrapie-infected mice. J. Clin. Invest. *116*, 3204–3210.

Prusiner, S.B. (1982). Novel proteinaceous infectious particles cause scrapie. Science *216*, 136–144.

Prusiner, S.B. (1998). Prions. Proc. Natl. Acad. Sci. USA *95*, 13363–13383.

Prusiner, S.B., Cochran, S.P., Groth, D.F., Downey, D.E., Bowman, K.A., and Martinez, H.M. (1982). Measurement of the scrapie agent using an incubation time interval assay. Ann. Neurol. *11*, 353–358.

Safar, J., Wille, H., Itri, V., Groth, D., Serban, H., Torchia, M., Cohen, F.E., and Prusiner, S.B. (1998). Eight prion strains have PrP(Sc) molecules with different conformations. Nat. Med. *4*, 1157–1165.

Santoro, M.M., and Bolen, D.W. (1988). Unfolding free energy changes determined by the linear extrapolation method. 1. Unfolding of phenylmethanesulfonyl alpha-chymotrypsin using different denaturants. Biochemistry *27*, 8063–8068.

Smirnovas, V., Baron, G.S., Offerdahl, D.K., Raymond, G.J., Caughey, B., and Surewicz, W.K. (2011). Structural organization of brain-derived mammalian prions examined by hydrogen-deuterium exchange. Nat. Struct. Mol. Biol. *18*, 504–506.

Vanik, D.L., and Surewicz, W.K. (2002). Disease-associated F198S mutation increases the propensity of the recombinant prion protein for conformational conversion to scrapie-like form. J. Biol. Chem. *277*, 49065–49070.

Wang, F., Wang, X., Yuan, C.G., and Ma, J. (2010). Generating a prion with bacterially expressed recombinant prion protein. Science *327*, 1132–1135.

Weissmann, C. (2004). The state of the prion. Nat. Rev. Microbiol. *2*, 861–871.

Westergard, L., Christensen, H.M., and Harris, D.A. (2007). The cellular prion protein (PrP(C)): its physiological function and role in disease. Biochim. Biophys. Acta *1772*, 629–644.

Yuan, X., Yao, J., Norris, D., Tran, D.D., Bram, R.J., Chen, G., and Luscher, B. (2008). Calcium-modulating cyclophilin ligand regulates membrane trafficking of postsynaptic GABA(A) receptors. Mol. Cell. Neurosci. *38*, 277–289.

Zahn, R., Liu, A., Lührs, T., Riek, R., von Schroetter, C., López García, F., Billeter, M., Calzolai, L., Wider, G., and Wüthrich, K. (2000). NMR solution structure of the human prion protein. Proc. Natl. Acad. Sci. USA *97*, 145–150.